Polarization-mode hopping in single-mode vertical-cavity surface-emitting lasers: Theory and experiment

Bob Nagler,[1,*] Michael Peeters,[1] Jan Albert,[1] Guy Verschaffelt,[1] Krassimir Panajotov,[1,†] Hugo Thienpont,[1] Irina Veretennicoff,[1] Jan Danckaert,[1] Sylvain Barbay,[2,‡] Giovanni Giacomelli,[2,3] and Francesco Marin[3,4]

[1]*Department of Applied Physics and Photonics, Vrije Universiteit Brussel, Pleinlaan 2, B-1050 Brussel, Belgium*

[2]*Instituto Nazionale di Ottica Applicata (INOA), Largo E. Fermi 6, 50125 Firenze, Italy*

[3]*INFM, Unità di Firenze, Firenze, Italy*

[4]*Dipartimento di Fisica and LENS, Università di Firenze, via Sansone 1, 50019 Sesto Fiorentino, Italy*

(Received 19 December 2002; published 15 July 2003)

In this paper, we present a theoretical and experimental analysis of stochastic effects observed in polarization switching vertical-cavity surface-emitting lasers. We make a thorough comparison between theoretical predictions and experiments, comparing measured quasipotentials and dwell times. The correspondence between our theoretical model based on stochastic intensity rate equations and the experiments is found to be very good.

DOI: 10.1103/PhysRevA.68.013813 PACS number(s): 42.60.Mi, 42.55.Px, 42.65.Sf, 42.50.−p

I. INTRODUCTION

Vertical-cavity surface-emitting lasers (VCSELs) have evolved in a very short time from laboratory curiosities [1] to highly successful optical sources, used in various applications. This has been possible because VCSELs outclass the traditional edge-emitting lasers in many different ways and are often a better choice in applications where high emission power is not required. They have an excellent beam profile (low divergence, circular shape), are very efficient, have a low lasing threshold (milliampere range is common), are intrinsically single-longitudinal mode, etc. Moreover, their structure allows for the fabrication of two-dimensional (2D) arrays and on-wafer testing, which reduces their mass-production cost significantly.

Since their conception, VCSELs have been studied extensively. Nevertheless, not all the physical mechanisms taking place inside these devices are completely understood. One of these remaining problems is their polarization behavior. Despite their cylindrical symmetry, VCSELs most often emit linearly polarized light along one of two particular crystallographic directions, [110] and [1-10] when the growth direction is along [001]. Moreover, in many VCSELs abrupt switching from one polarization mode (PM) to the other is observed when the injected current is changed. Of particular concern in this paper is the polarization mode hopping that occurs when a free standing VCSEL is biased close to the polarization switching current. The VCSEL then switches in a random fashion between the two PMs [2–4]. The average time between consecutive switches varies over several orders of magnitude, from nanoseconds when the polarization switching (PS) occurs close to lasing threshold to several seconds at higher currents. Also in current driven polarization modulation stochastic effects play an important role [5–9]. The stochastic polarization properties of VCSELs under feedback [10–12] and optical injection [13] have drawn a lot of attention too.

In this work, we present ample experimental data obtained on different kinds of VCSELs, both index and gain guided. These data are then compared with theoretical results based on a two-mode rate equation model [14] adapted to describe the polarization behavior of VCSELs [15]. Not only the switching time [16] and the scaling of the average residence times [2–4], but also the residence time distribution and quasipotentials are quantitatively compared with theoretical results. Our theory is based on an asymptotic analysis of stochastic intensity rate equations for a two-mode semiconductor laser. First, taking advantage of the different time scales present in the model, the original set of three equations is reduced to one single dynamical equation for one of the intensities. Then the Kramers theory for hopping in a two-well potential can be applied [17]. In order to test all the approximations made in the analytical treatment, the analytical results are compared with numerical simulations obtained from the original set of equations. The agreement is found to be very good. In this way, we also validate that analytical techniques such as a multiple time scale analysis, often applied to simplify deterministic equations, can also be applied to stochastic rate equations [18,19].

Polarization instability is a great nuisance in many applications where polarization sensitive components are used. It is therefore not only interesting from a fundamental point of view, but also of great practical importance to understand the physics of PS in VCSELs. This should ultimately lead to techniques for stabilizing the polarization state [20]. Alternatively, one could actively control the PS to exploit the extra degrees of freedom offered by the polarization state of the light [21].

The following section starts with an overview of the different models that have been proposed to describe PS in VCSELs. We derive analytical expressions, based on the Kramers theory, which predict the polarization mode-hopping statistics. These results are compared with numeri-

*Electronic address: Bob.Nagler@vub.ac.be; URL: http://www.tona.vub.ac.be

†Permanent address: Institute of Solid State Physics, 72 Tzarigradsko Chaussee Blvd., 1784 Sofia, Bulgaria.

‡Present address: Laboratoire de Photonique et de Nanostructures, CNRS–UPR 20, Route de Nozay, 91460 Marcoussis, France.

cal simulations and verified against ample experimental data, obtained with both gain- and index-guided VCSELs.

II. STOCHASTIC RATE EQUATIONS

Our theoretical starting point will be a standard intensity rate equation model for a two-mode semiconductor laser: two equations for the optical intensities in each of the PMs and one for the carrier population inversion. Such rate equations have been widely used to study the properties of a two-mode semiconductor laser [14,15,22–25]. However, in VCSELs, the situation is peculiar as it was pointed out that carrier spin dynamics in the active layer of the semiconductor material could play a role [26], especially with respect to the polarization behavior. The spin-flip model (SFM) [26] is describing the field-matter interaction in terms of a spin-split two-level model [27–31]. The original SFM consists of four equations: two for the complex fields and two for the carrier inversions in each of the spin channels. A considerable effort has been made to simplify the original SFM equations in order to obtain more insight [4,32–34]. It was proven theoretically [4,33,34] that the SFM equations can be reduced to standard intensity rate equations for a semiconductor laser under the following assumptions: (i) a relatively large spin-flip rate ($>50\ \mathrm{ns}^{-1}$), so that the population difference between the spin channels can be eliminated and (ii) a relatively large birefringence (>1 GHz), so that fast beating oscillations due to the frequency difference between the two modes can be averaged. The remnants of the spin difference can then be found in nonzero cross-saturation coefficients between the two PMs. We have no direct experimental evidence of the spin-flip rate from our experiments, but we assume it to be larger than the above-mentioned value. This is motivated by the fact that we have not observed strong multiply peaked spectra close to the PS current that are typical of strong nonlinearities such as spin flips [35]. We do have experimental measurements of the birefringence in our VCSELs, and, although birefringence through our experiments varies with strain, it is always of the order of 10 GHz. That is why, to explain our experimental results reported in Sec. IV, we can safely apply a two-mode intensity rate equation model with gain saturation. Polarization switching in this model is obtained by a phenomenological dependence of the gain-loss difference between the two modes (dichroism) on parameters such as the injected current and/or temperature [15,33].

We propose a rate equation model for photon densities in the the x and y polarization modes P_x and P_y, and the carrier density N as in Ref. [15]. The gain is current dependent, linear in the carrier inversion and saturates with increasing optical power. In each equation, we add a white-noise term $\tilde{F}'_{x,y,N}$. The equations read

$$\frac{dP_x}{dt'}=[\Gamma_x a_x(N-N_t)(1-e_{sx}P_x-e_{xy}P_y)-\tau_{px}^{-1}] + \beta_{sp,x}N+\tilde{F}'_x, \tag{1}$$

$$\frac{dP_y}{dt'}=[\Gamma_y a_y(N-N_t)(1-e_{sy}P_y-e_{yx}P_x)-\tau_{py}^{-1}] + \beta_{sp,y}N+\tilde{F}'_y, \tag{2}$$

$$\frac{dN}{dt'}=\frac{I}{q_e V}-\frac{N}{\tau_c}-a_x(N-N_t)(1-e_{sx}P_x-e_{xy}P_y)P_x - a_y(N-N_t)(1-e_{sy}P_y-e_{yx}P_x)P_y+\tilde{F}'_N. \tag{3}$$

All the stochastic differential equations have to be interpreted in the Stratonovich sense [36]. The autocorrelation of the noise is given by [36]

$$\langle\tilde{F}'_x(t)\tilde{F}'_x(s)\rangle=4\beta_{sp,x}Np_x\delta(t-s), \tag{4}$$

$$\langle\tilde{F}'_y(t)\tilde{F}'_y(s)\rangle=4\beta_{sp,y}Np_y\delta(t-s), \tag{5}$$

$$\langle\tilde{F}'_x(t)\tilde{F}'_y(s)\rangle=0. \tag{6}$$

Here, $e_{sy,sx,xy,yx}$, $\Gamma_{x,y}$, $a_{x,y}$, $\tau_{px,y,}$ and $\beta_{sp,x,y}$ represent the saturation coefficients, confinement factors, the gain coefficients, the photon lifetimes, and the noise strength for each mode, respectively. In the carrier equation, I, q_e, V are the injected current, the elementary charge, and the volume of the active region. As in Refs. [15,37], we reduce these equations, taking advantage of the different time scales present in the model and the fact that the PMs in a VCSEL are nearly degenerate and have nearly equal parameters [15,37]:

$$\frac{dp_x}{dt}=p_x[\eta-\varepsilon_{sx}p_x-\varepsilon_{xy}p_y]+\frac{1}{2}R_{sp}+\tilde{F}_x, \tag{7}$$

$$\frac{dp_y}{dt}=p_y[\eta+G(J)-\varepsilon_{sy}p_y-\varepsilon_{yx}p_x]+\frac{1}{2}R_{sp}+\tilde{F}_y, \tag{8}$$

$$\frac{d\eta}{dt}=\frac{J-p_x-p_y}{\rho}-\eta-p_x[\eta-\varepsilon_{sx}p_x-\varepsilon_{xy}p_y] - p_y[\eta-\varepsilon_{sy}p_y-\varepsilon_{yx}p_x]+\tilde{F}_n. \tag{9}$$

The time t is reduced with respect to the carrier lifetime (i.e., nanoseconds), and $\rho=(\tau_p/\tau_c)\simeq 10^{-3}$. The dynamical variables p_x, p_y are the reduced photon densities, while η is the deviation of the carrier density from its clamped value above threshold. The parameters J, $\varepsilon_{sx,sy,xy,yx}$, and $G(J)=\rho^{-1}(\tau_{py}\Gamma_y a_y-\tau_{px}\Gamma_x a_x)/\tau_{px}\Gamma_x a_x$ are the reduced current, saturation coefficients, and current dependent dichroism, while $R_{sp}=\rho^{-1}(2\tau_c/\Gamma_x)(1+\tau_{px}\Gamma_x a_x N_t)\beta_{sp,x}$ describes the mean of the spontaneous emission above threshold. The reduced noise terms are defined by

$$\tilde{F}_{x,y}=\tau_c^2 a_{x,y}\tilde{F}'_{x,y}, \tag{10}$$

$$\tilde{F}_\eta=\Gamma_x\tau_c^2 a_x\tilde{F}'_N, \tag{11}$$

with correlation functions:

$$\langle \tilde{F}_x'(t)\tilde{F}_x'(s)\rangle = 2R_{sp}p_x\delta(t-s), \tag{12}$$

$$\langle \tilde{F}_y'(t)\tilde{F}_y'(s)\rangle = 2R_{sp}p_y\delta(t-s), \tag{13}$$

$$\langle \tilde{F}_x'(t)\tilde{F}_y'(s)\rangle = 0. \tag{14}$$

In a next step, we further reduce Eqs. (7)–(9), using the same approach as in Refs. [15,37]. To leading order in ρ, Eq. (9) yields a conservation relation, stating that the total photon density equals the reduced current above threshold:

$$p_x + p_y = J. \tag{15}$$

This equation implies that the fluctuation of the photon densities in both modes are anti-correlated, as is indeed experimentally observed [2,3]. Taking the time derivative of Eq. (15) and substituting Eq. (15) and Eqs. (7) and (8), yields an expression for the carrier inversion for a constant current:

$$\eta = \frac{1}{J}\{\Delta p_y^2 + [(\varepsilon_{xy}+\varepsilon_{yx}-2\varepsilon_{sx})J - G]p_y + \varepsilon_{sx}J^2 - R_{sp} - \tilde{F}_x - \tilde{F}_y\}, \tag{16}$$

where Δ is defined by

$$\Delta = \varepsilon_{sx}+\varepsilon_{sy}-\varepsilon_{xy}-\varepsilon_{yx}. \tag{17}$$

Substitution of Eqs. (16) and (15) in Eq. (8), yields a single dynamical equation:

$$\dot{p}_y = C(p_y) + \tilde{F}(p_y), \tag{18}$$

with a deterministic drift term

$$C(p_y) = p_y(J-p_y)\left(-\frac{\Delta}{J}p_y + \varepsilon_{sx} - \varepsilon_{yx} + \frac{G}{J}\right) + \frac{R_{sp}}{2J}(J-2p_y), \tag{19}$$

and a stochastic term

$$\tilde{F}(p_y) = \tilde{F}_y - \frac{\tilde{F}_x+\tilde{F}_y}{J}p_y. \tag{20}$$

Equation (18) describes the dynamics of the system on the time scale of our reduction (i.e., the carrier lifetime) and slower. Faster dynamics, such as the relaxation oscillations, are no longer present in our one-dimensional reduction.

The stationary solutions of these equation can be found in Refs. [15,37]. We briefly summarize these results here. When the spontaneous emission is neglected (i.e., $R_{sp}=0$), Eqs. (18) and (19) clearly show that two kinds of lasing solutions exist: two pure mode solutions ($p_x \simeq 0$, $p_y \simeq J$ and $p_x \simeq J$, $p_y \simeq 0$) and a mixed mode solution ($p_x \simeq (\varepsilon_{sy}-\varepsilon_{xy})J - G/\Delta, p_y \simeq [(\varepsilon_{sx}-\varepsilon_{yx})J+G]/\Delta$). Linear stability analysis shows [15,37] that the stability of the pure mode solutions changes around the point where $G(J)=0$. If $\Delta<0$, the two pure mode solutions coexist in a region of bistability and the mixed mode solution is unstable. This condition is equivalent to supposing that the cross mode gains saturation is larger than the self-saturation. Such a situation is indeed found in a reduction of the SFM model [34,38], and also by considering band-scattering effects [39].

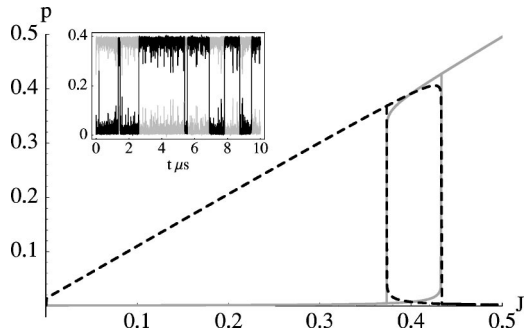

FIG. 1. Numerical solution of Eqs. (7)–(9) with a ramping current. There is a region of bistability. Parameter values (corresponding to the index-guide devices of the experiments) are $\varepsilon_{sx}=\varepsilon_{sy}=4$, $\varepsilon_{xy}=\varepsilon_{yx}=8$, $G(J)=g(1-J/J_s)$ with $g=14$, $J_s=0.4$, $R_{sp}=0.023$, $\rho=10^{-3}$. The inset is a numerical time trace in the middle of the bistable region at $J=J_s=0.4$.

The stable steady-state solutions can be seen in the simulation shown in Fig. 1. We will call the mode which starts lasing at threshold the p_y mode. This implies that $G(J)$ is positive at threshold and decreases with increasing current.

If the current is modulated across the bistable region, a switch is observed between the modes. The deterministic switching time can be derived analytically [15] and is primarily determined by the photon lifetime and the relative net gain difference between the two modes. The magnitude of gain differences have been measured to be of the order of 10^{-3} or less [40]. For this value, we have a switching time (10% to 90%) of the order of 10 ns [15], which matches the deterministic switching time recorded in modulation experiments [5].

III. FIRST PASSAGE TIMES AND MODE HOPPING

In the bistable region where the two pure mode solutions are stable (see Fig. 1), random hops can occur due to spontaneous emission noise. Such stochastic transitions between two stable solutions can be treated as a first passage time problem over a potential barrier [41,36]. This has been done in the past to explain stochastic switching in other kinds of lasers [42–45] and other systems [2–4,46]. We apply this technique to our dynamical equation (18). This approach will lead to an expression for the so-called quasipotential, which can be compared with our experimental results.

Due to spontaneous emission noise, the intensity p_y in Eq. (18) is a stochastic variable (from now on, we denote p_y as p). The probability density function $\mathcal{P}(p,t)$ of the intensity changes in time according to the following Fokker-Planck equation [47]:

$$\frac{\partial \mathcal{P}(p,t)}{\partial t} = -\frac{\partial}{\partial p}[A(p)\mathcal{P}(p,t)] + \frac{\partial^2}{\partial p^2}[D(p)\mathcal{P}(p,t)], \tag{21}$$

where

$$\langle \tilde{F}(p,t_1),\tilde{F}(p,t_2)\rangle = 2D(p)\,\delta(t_1-t_2), \tag{22}$$

with the diffusion coefficient given by [using Eq. (20)]

$$D=\frac{R_{sp}}{J}p(J-p). \tag{23}$$

The drift coefficient is given by [using Eq. (19)]

$$A(p)=C(p)+\frac{1}{2}\frac{dD(p)}{dp} \tag{24}$$

$$=p(J-p)\left(-\frac{\Delta}{J}p+\varepsilon_{sx}-\varepsilon_{yx}+\frac{G}{J}\right)+\frac{R_{sp}}{J}(J-2p). \tag{25}$$

The stationary solution of the Fokker-Planck equation (21) is

$$\mathcal{P}_s(p)=Qe^{-U(p)}, \tag{26}$$

with Q a normalization coefficient and quasipotential $U(p)$ given by

$$U(p)=-\int\frac{C(p)}{D(p)}dp+\frac{1}{2}\ln[D(p)] \tag{27}$$

$$=\frac{\Delta}{2R_{sp}}p^2+\frac{1}{R_{sp}}[(\varepsilon_{yx}-\varepsilon_{sx})J-G]p. \tag{28}$$

From now on, we will assume that

$$\varepsilon_{xy}-\varepsilon_{sy}=\varepsilon_{yx}-\varepsilon_{sx}=\delta, \tag{29}$$

since this is expected due to the symmetric VCSEL structure. We will limit ourselves to the symmetric case, when there is no linear dichroism between the two modes [i.e., $G(J)=0$], and the devices spends an equal amount of time in each mode. The potential then has the elegant form

$$U(p)=\frac{\delta}{R_{sp}}p(J-p). \tag{30}$$

Note that this potential is only valid for $0<p<J$. This is implied by Eq. (15), and due to the multiple time-scale analysis.

Equation (26) is known as the potential solution. Quasipotentials for a bias current in the middle of the bistable region are shown in Sec. III B and compared with numerical ones. The physical significance of the quasipotential will become clear when we derive the expression for the dwell time in the following section.

A. Dwell time

We now derive the mean time it takes for the laser to hop from one mode to the other. The general theory is explained in Ref. [41], so we only summarize the specific results in the framework of our model.

To hop from one stable mode to the other, the laser has to cross a potential barrier (associated with the unstable solution) : the spontaneous emission noise has to ''kick'' the laser out of the basin of attraction of one stationary solution into the other. The time the system resides in one stable mode before switching to the other is called the residence time or first passage time. This time is itself a stochastic variable with an exponential distribution [41]

$$\mathcal{P}(t)=\frac{1}{t_{dw}}\exp\left(-\frac{t}{t_{dw}}\right). \tag{31}$$

The mean time the system takes to hop between the modes, t_{dw}, is called the dwell time. It can be calculated using the stationary solution of the Fokker-Planck equation [36,41]:

$$t_{dw}=2D(p_{\max})^{-1}\int_0^{p_{\max}}\mathcal{P}_s(p)dp\int_0^{p_{\max}}\mathcal{P}_s(p)^{-1}dp, \tag{32}$$

where $p_{\max}$ is the intensity for which the potential attains it maximum. For the symmetric potential (30), we have $p_{\max}=J/2$, and using Eq. (26), (30), and (32), we find [54]

$$t_{dw}=\frac{2\pi}{J\delta}\mathrm{erf}\left(\frac{J}{2}\sqrt{\frac{\delta}{R_{sp}}}\right)\mathrm{erfi}\left(\frac{J}{2}\sqrt{\frac{\delta}{R_{sp}}}\right). \tag{33}$$

If we use an asymptotic series expansion of the error functions, we get

$$t_{dw}=\frac{4}{J^2}\sqrt{\frac{\pi R_{sp}}{\delta^3}}\exp\left(\frac{J^2\delta}{4R_{sp}}\right). \tag{34}$$

This equation is equivalent with Eq. (20) in Ref. [33].

Expressions (30) for the quasipotential and (33) for the dwell time are the main theoretical results of this paper, and can be compared with experimental results, as we will show later. First, we will proceed with the numerical verification of our theoretical results.

B. Numerical verification of the reductions

To verify the validity of the one-dimensional reduction, and the subsequent analytical derivation of the dwell time, we performed numerical simulations. We used a C++ template class framework, which is freely available [48], developed to address shortcomings (such as the absence of built-in stochastic integration and low integration speed) in standard packages (e.g., MATHEMATICA). The rate equation system (or any system of ordinary differential equations) is specified as a particular specialization of a single class.

We solved Eqs. (7)–(9) numerically with a second-order stochastic corrector-predictor integrator (often called the Heun algorithm) converging to the Stratonovich solution as required. At the same time, the reduced 1D equation (18) was also integrated to assert the validity of the reduction. The constant current was set in the middle of the bistable region, where the gain difference is zero. A typical mode-hopping trace can be seen in the inset of Fig. 1.

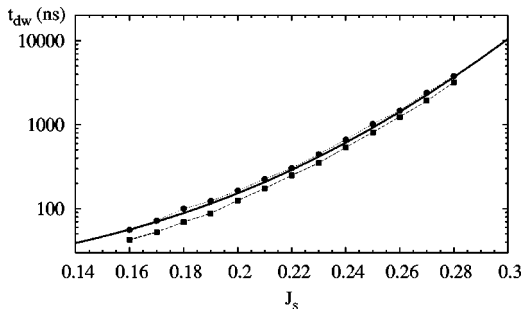

FIG. 2. Comparison between the dwell times of the numerical simulations of the three-dimensional model [Eqs. (7)–(9), black squares], the one-dimensional model [Eq. (18), hollow circles], and the analytical prediction [Eq. (33), full line]. Same parameter values as in Fig. 3.

We obtained the dwell times from the traces by taking the average of the residence time over a thousand switches. Similar as in the experimental procedure, we have defined a successful switch to be one where the system has crossed 80% of the interval between its lasing and nonlasing state. This avoids defining a deterministic crossing point.

This was repeated for different switching current values. The resulting curve, dwell time as a function of switching current, is compared in Fig. 2 with the analytical prediction, Eq. (33), for parameter values corresponding to our gain-guided VCSELs. The match between the theory and numerics is perfect for the 1D case. The 3D simulations show a slightly smaller (15%) average dwell time, predominantly close to threshold. This difference diminishes with increasing switching current and is related to the fact that the noise is not filtered by the reduction. Repeating the procedure for parameters corresponding to the index-guided case, we come to the same conclusions.

We obtained the 1D potential by numerically integrating Eq. (18) and taking the histogram of the time trace, which we compared with the theoretical predictions in Fig. 3. Although they match exactly, it is impossible to compare these potentials to the experiments, as the presence of a detector with a finite bandwidth implies that we are measuring a time-

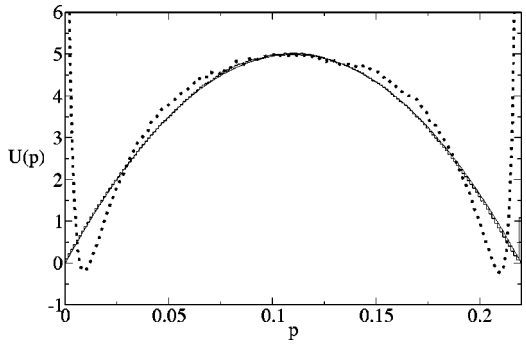

FIG. 3. Comparison between the numerical integration of Eq. (18) (steps) and the analytical prediction (30) (full line). The two curves are difficult to distinguish as they overlap well. The effect of the first-order time response of the detector on the potential is shown by the dotted curve. Parameter values are $\delta=4.23$, $J=0.22$, and $R=0.01$.

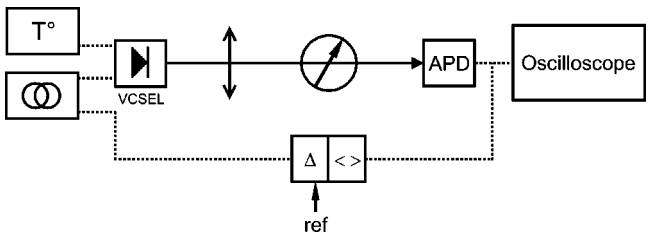

FIG. 4. Scheme of the experimental setup.

averaged output power. It is well known [36] that the probability density function (pdf) of such a quantity is different from the original pdf, as can be seen in Fig. 3. Indeed, this problem often appears in quantum optics when studying the fluctuations of the electromagnetic field of a laser with a nonideal detector. Although analytical methods exist to compute the pdf of the time-averaged version from the original pdf, these do not directly lead to a closed-form solution in our case. Therefore, we have compared the experimentally recorded pdf's of the intensity with numerical ones, incorporating the first-order time response of the detector into the simulations.

IV. EXPERIMENTS

We have performed an elaborate statistical analysis of the polarization mode-hopping characteristics of both proton-implanted and air-post VCSELs. Earlier measurements on the devices under test [49] have shown that the frequency splitting between the two polarization modes is of the order of 10 GHz. By applying mechanical stress to the VCSEL package, we can tune the polarization switching current over a wide range. For the different switching currents, we have recorded and analyzed mode-hopping time series. We have determined the average residence time (or dwell time) and verified its dependence on the switching current against the theoretical prediction. Moreover, we have studied the intensity histograms. These, as will be explained below, are directly linked with the quasipotentials and will be compared with numerical simulations. This cross validation was, to our knowledge, never performed before and is a confirmation of the validity of the model, in general, and the treatment of polarization mode hopping as a Kramers problem in particular.

A. The measurements

The scheme of the experimental setup is shown in Fig. 4. The temperature controller and the laser driver are in-house made components. The 1-GHz oscilloscope (Lecroy) has built-in functions for on-line statistical analysis. We drive the VCSEL with a constant current in the middle of the bistable region. The light is sent through a 5-cm focal-length lens and focused onto the small detector, an avalanche photodiode (APD) with a bandwidth of over 1 GHz. A polarizer selects the polarization state. All the optics are slightly misaligned in order to avoid optical feedback, which is known to induce extra instabilities and affect the dynamical time scales. Within the resolution of our Fabry-Perot spectrum analyzer

no traces of feedback were present in the spectrum. Also the switching conditions and the mode-hopping dynamics were stable under small variations of the misalignment angle. Moreover the setup was robust against acoustic vibrations. From this, we conclude that optical feedback was successfully eliminated.

The oscilloscope records time series and readily calculates histograms of the intensity and of the time lapses spent in each PM, together with the average length of these lapses. To tune the PS current with respect to the threshold current, the VCSEL is mounted in a specially designed holder with which we can induce uniaxial strain in the VCSEL package [20]. By varying the strength and the direction of the strain, we are able to tune the reduced current J in the range between 0.15 and 0.8.

To allow for comparison with the theory, it is essential that the symmetry of the two-well potential is maintained. For this purpose, the driving current must be fixed exactly in the middle of the bistable region. Therefore, we introduced a locking feedback loop: the averaged output signal of the APD is compared with an adjustable reference value. The error signal is integrated and fed back to the VCSEL with a loop bandwidth of about 10 Hz. Careful adjustment of the reference value allows us to lock the VCSEL exactly in the middle of its bistable region.

We performed our measurements on two different types of VCSELs. First, a proton implanted (gain guided) GaAs/AlGaAs VCSEL from VIXEL Corporation, operating around 850 nm with a threshold of about 7 mA. As it is a commercial device, we have no positive information about its structure. From the literature [50], however, we guess that the device structure contains 3-GaAs quantum wells of 8 nm thickness centered in a 1λ cavity with a 29.5 pair *n*-doped bottom DBR (distributed Bragg reflector) and a 19 pair *p*-doped top DBR. The cavity diameter is 8 μm. Contrary to similar VCSELs on which mode-hopping experiments have been reported [4], our devices show polarization switching from lower to higher frequency with increasing current (i.e., type-II switching [51]). Second, an air-post- (index guided) type VCSEL from Avalon Photonics (former CSEM), operating around 980 nm with a threshold of about 3.3 mA. The device has three 8-nm-thick GaInAs QWs embedded in 10-nm-thick GaAs barriers and has GaAs/AlGaAs mirrors. In these devices we observe type-I PS. It was shown [52] that polarization switching in the gain-guided devices is primarily of thermal origin, while the index-guided devices exhibit nonthermal switches [53].

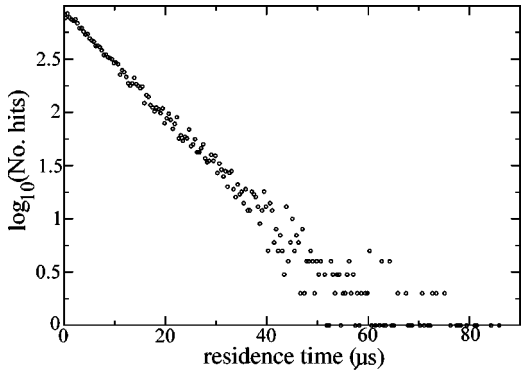

FIG. 5. Example of a measured exponential distribution of the residence time of an air-post VCSEL at $J=0.4$.

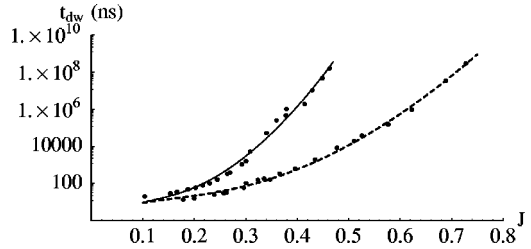

FIG. 6. Dwell time as a function of the switching current, for the air-post (dashed line) and the proton-implanted (solid line) devices. The measurements (dots) are fitted with Eq. (33), the parameter values of the fit are in Table I.

B. The results

Throughout the measurements, we can limit ourselves to analyzing the mode-hopping dynamics of one of the polarization states, since the other polarization state shows complementary dynamics.

For different values of the reduced current J, we have recorded an intensity histogram of the polarization mode hopping as well as a residence time histogram. An example of the latter is presented in Fig. 5. It was recorded on the air-post device. The corresponding average residence time is 9.5 μs. The exponentially decreasing distribution of the residence times, as predicted by Arrhenius' law—Eq. (31)—can clearly be seen.

In this case, the Kramers time, i.e., the characteristic time of the exponential function, coincides with the mean residence time. This property is well verified on the whole range of experimental parameters. We can thus identify the measured mean residence time t_{dw} with the Kramers time.

We use the logarithm of Eq. (33) as a fitting function for t_{dw} versus J, a theoretical expression with only two free parameters, namely, δ and R_{sp}.

In Fig. 6, we report the measured values of t_{dw} as a function of J, together with the fitting curves. The fit is excellent and the extracted parameters are reported in Table I.

At the same time, one can see from Eq. (26) that the inverse of the logarithm of the polarized intensity histograms gives the quasipotential $U(p)$. Equation (30) shows that in the symmetric case (i.e., in the middle of the bistable region where $G=0$), the quasipotential only depends on δ and R_{sp}

TABLE I. Fitting parameter values of Eq. (33) with experimental data, as shown in Fig. 6.

VCSEL	δ	R_{sp}
Proton implanted	8.5	0.022
Air post	3.4	0.022

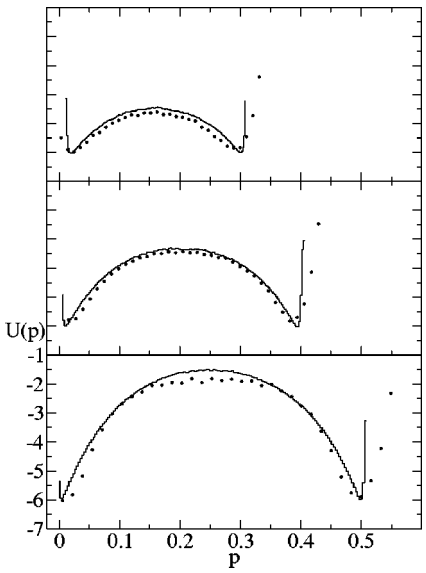

FIG. 7. Comparison of experimentally obtained quasipotentials (dots) with numerical simulations (full line). A first-order filter with a time constant of 0.125 ns is included in the simulations to mimic the detector. The switching current increases from top to bottom (a) $J_s=0.3$, (b) $J_s=0.4$, (c) $J_s=0.5$). The values of δ and R_{sp} are taken from the fit of dwell times—see Table I.

(besides the switching current J, which is an input variable). The measured intensity histograms thus allow us to cross-check the obtained fitting values for δ and R_{sp}. However, one has to be careful: Eq. (30) only takes into account the average value of the spontaneous emission noise and disregards high-frequency intensity fluctuations. For a proper verification of the measured quasipotentials, one has to compare them with a stochastic numerical simulation that also takes the bandwidth limit of the detector into account, as was explained in Sec. III B. In Fig. 7, we show the comparison between the experimentally measured quasipotentials for different values of the switching current J and the ones obtained by numerical simulation, using the fitted values of δ and R_{sp} and a detector time constant of 0.125 ns. For the sake of brevity, we only show the results of the air-post device. The excellent agreement is a confirmation of the validity of the model, in general, and the treatment of polarization mode hopping as a Kramers problem in particular.

V. SUMMARY

We have presented a thorough experimental and theoretical investigation of the polarization mode hopping in VCSELs. The theoretical starting point is a set of intensity rate equations for a semiconductor laser with two nearly degenerate modes including self- and cross-gain saturation. Taking advantage of the different time scales in these equations, they can be reduced to a single dynamical equation, which is only valid on time scales slower than the relaxation oscillations. From this dynamical equation, the intensity statistics and the quasipotentials can be derived. Analytical expressions for the scaling of the average residence time with the PS current can be derived, applying Kramers' theory for hopping in a two-well potential. These results are checked by comparing the analytical expressions with results from the numerical simulations. The agreement is found to be very good, validating the multiple time-scale analysis and the application of Kramers' theory.

The theoretical results are then compared with ample measurements, on two different kinds of VCSELs (gain and index guided), that show different types of switching (from higher to lower frequency and vice versa) of different origins (thermal and nonthermal). In both cases, the agreement between theory and experiment is found to be very good. We compare probability density function of the intensity, which is directly linked with the quasipotential, and the average residence times with theory. In this way, we establish that our original stochastic intensity rate equations and the subsequent reduction based on a multiple time-scale analysis describe the mode-hopping statistics well in both types of devices.

ACKNOWLEDGMENTS

This research was supported by the Belgian Office for Scientific, Technical and Cultural Affairs in the framework of the Interuniversity Attraction Pole Program, the Fund for Scientific Research—Flanders (FWO), the Concerted Research Action ''Photonics in Computing,'' and the research council (OZR) of the Vrije Universiteit Brussel. B.N., G.V., and J.D. acknowledge the FWO for financial support. J.A. acknowledges the Institute for Scientific-Technological Research (IWT). The collaboration between the groups was supported by EU programs COST268 and the RTN network VISTA (Contract No. HPRN-CT-2000-00034).

[1] H. Soda, K. Iga, C. Kitahara, and Y. Suematsu, Jpn. J. Appl. Phys. **18**, 2329 (1979).
[2] G. Giacomelli and F. Marin, Quantum Semiclassic. Opt. **10**, 469 (1998).
[3] G. Giacomelli, F. Marin, M. Gabrysch, K.H. Gulden, and M. Moser, Opt. Commun. **146**, 136 (1998).
[4] M.B. Willemsen, M.U.F. Khalid, M.P. van Exter, and J.P. Woerdman, Phys. Rev. Lett. **82**, 4815 (1999).
[5] G. Verschaffelt *et al.*, Proc. SPIE **3946**, 246 (2000).
[6] G. Verschaffelt, J. Albert, B. Nagler, M. Peeters, J. Danckaert, S. Barbay, G. Giacomelli, and F. Marin (unpublished).
[7] S. Barbay, G. Giacomelli, and F. Marin, Phys. Rev. E **61**, 157 (2000).
[8] G. Giacomelli, F. Marin, and I. Rabbiosi, Phys. Rev. Lett. **82**, 675 (1999).
[9] B. Nagler, M. Peeters, J. Danckaert, and I. Veretennicoff, Phys. Rev. E **67**, 056112 (2003).
[10] P. Besnard, M.L. Chares, G. Stéphan, and F. Robert, J. Opt. Soc. Am. B **16**, 1059 (1999).
[11] P. Besnard, F. Robert, M. Chares, and G.M. Stéphan, Phys.

Rev. A **56**, 3191 (1997).
[12] J. Mork, B. Tromborg, and J. Mark, IEEE J. Quantum Electron. **28**, 93 (1992).
[13] Y. Hong, P.S. Spencer, S. Bandyopadhyay, P. Rees, and A. Shore, Opt. Commun. **216**, 165 (2003).
[14] Y.C. Chen and J.M. Liu, Appl. Phys. Lett. **50**, 1406 (1987).
[15] J. Danckaert, B. Nagler, J. Albert, K. Panajotov, I. Veretennicoff, and T. Erneux, Opt. Commun. **201**, 129 (2002).
[16] M.B. Willemsen, M.P. van Exter, and J.P. Woerdman, Phys. Rev. Lett. **84**, 4337 (2000).
[17] H.A. Kramers, Physica (Utrecht) **7**, 284 (1940).
[18] P. Jung and P. Hänggi, Phys. Rev. A **35**, 4464 (1987).
[19] P. Hänggi and P. Riseborough, Am. J. Phys. **51**, 347 (1983).
[20] K. Panajotov, B. Nagler, G. Verschaffelt, A. Georgievsky, H. Thienpont, J. Danckaert, and I. Veretennicoff, Appl. Phys. Lett. **77**, 1590 (2000).
[21] N. Nieuborg, K. Panajotov, I. Veretennicoff, and H. Thienpont, IEEE Photonics Technol. Lett. **10**, 973 (1998).
[22] G.P. Agrawal, Phys. Rev. A **37**, 2488 (1988).
[23] H. Kawaguchi, I.H. White, M.J. Offside, and J.E. Carroll, Opt. Lett. **17**, 130 (1992).
[24] M. Okada and K. Nishio, IEEE J. Quantum Electron. **32**, 1767 (1996).
[25] H. Kawaguchi, IEEE J. Sel. Top. Quantum Electron. **3**, 1254 (1997).
[26] M. San Miguel, Q. Feng, and J.V. Moloney, Phys. Rev. A **52**, 1728 (1995).
[27] J. Martin-Regalado, M. San Miguel, N.B. Abraham, and F. Prati, Opt. Lett. **21**, 351 (1996).
[28] J. Martin-Regalado, F. Prati, M. San Miguel, and N.B. Abraham, IEEE J. Quantum Electron. **33**, 765 (1997).
[29] J. Martin-Regalado, J.L.A. Chilla, J.J. Rocco, and P. Brusenbach, Appl. Phys. Lett. **70**, 3350 (1997).
[30] S. Balle, E. Tolkachova, M.S. Michel, J.R. Tredicce, J. Martin-Regalado, and A. Gahl, Opt. Lett. **24**, 1121 (1999).
[31] J. Mulet and S. Balle, Int. J. Quantum Chem. **38**, 291 (2002).
[32] T. Erneux, J. Danckaert, K. Panajotov, and I. Veretennicoff, Phys. Rev. A **59**, 4660 (1999).
[33] M.P. van Exter, M.B. Willemsen, and J.P. Woerdman, Phys. Rev. A **58**, 4191 (1998).
[34] G. Van der Sande, J. Danckaert, I. Veretennicoff, and T. Erneux, Phys. Rev. A **67**, 013809 (2003).
[35] T. Ackemann and M. Sondermann, Appl. Phys. Lett. **78**, 3574 (2001).
[36] H. Risken, *The Fokker-Planck Equation* (Springer-Verlag, Berlin, 1996).
[37] B. Nagler, J. Danckaert, J. Albert, M. Peeters, K. Panajotov, I. Veretennicoff, and T. Erneux, Proc. SPIE **4283**, 275 (2001).
[38] M.P. van Exter, M.B. Willemsen, and J.P. Woerdman, J. Opt. B: Quantum Semiclassical Opt. **1**, 637 (1999).
[39] B.M. Yu and J.M. Liu, J. Appl. Phys. **69**, 7444 (1991).
[40] M.P. van Exter, M.B. Willemsen, and J.P. Woerdman, Proc. SPIE **3946**, 58 (2000).
[41] C.W. Gardiner, *Handbook of Stochastic Methods for Physics and Natural Sciences* (Springer-Verlag, Berlin, 1983).
[42] F.T. Hioe, S. Singh, and L. Mandel, Phys. Rev. A **19**, 2036 (1979).
[43] R. Roy, R. Short, J. Durnin, and L. Mandel, Phys. Rev. Lett. **45**, 1486 (1980).
[44] P. Lett, W. Christian, S. Singh, and L. Mandel, Phys. Rev. Lett. **47**, 1892 (1981).
[45] D. Lenstra and S. Singh, Phys. Rev. A **28**, 2318 (1983).
[46] M. Ohtsu, Y. Teramachi, Y. Otsuka, and A. Osaki, IEEE J. Quantum Electron. **22**, 535 (1986).
[47] M. Lax, Rev. Mod. Phys. **38**, 541 (1966).
[48] M. Peeters, http://model.sourceforge.net
[49] G. Verschaffelt, K. Panajotov, J. Albert, B. Nagler, M. Peeters, J. Danckaert, I. Veretennicoff, and H. Thienpont, Opto-Electron. Rev. **9**, 257 (2001).
[50] M.P. van Exter, A. Al-Remawi, and J.P. Woerdman, Phys. Rev. Lett. **80**, 4875 (1998).
[51] B. Ryvkin, K. Panajotov, A. Georgievski, J. Danckaert, M. Peeters, G. Verschaffelt, H. Thienpont, and I. Veretennicoff, J. Opt. Soc. Am. B **16**, 2106 (1999).
[52] G. Verschaffelt, J. Albert, I. Veretennicoff, J. Danckaert, S. Barbay, G. Giacomelli, and F. Marin, Appl. Phys. Lett. **80**, 2248 (2002).
[53] G. Verschaffelt *et al.*, Proc. SPIE **4649**, 245 (2002).
[54] The error function and the imaginary error function are defined by $\mathrm{erf}(x)=(2/\sqrt{\pi})\int_0^x e^{-t^2}dt$ and $\mathrm{erfi}(x)=-i\,\mathrm{erf}(ix)$.